First-principles investigation of chemical and structural disorder in magnetic $Ni_2Mn_{1+x}Sn_{1-x}$ Heusler alloys

V. V. Sokolovskiy,[1,2] V. D. Buchelnikov,[1] M. A. Zagrebin,[1] P. Entel,[3] S. Sahoo,[3,4] and M. Ogura[5]

[1]*Condensed Matter Physics Department, Chelyabinsk State University, 454001 Chelyabinsk, Russia*

[2]*National University of Science and Technology "MISiS," 119049 Moscow, Russia*

[3]*Faculty of Physics and Center for Nanointegration, CENIDE, University of Duisburg-Essen, D-47048 Duisburg, Germany*

[4]*Chemical Sciences and Engineering Division, Argonne National Laboratory, Argonne, Illinois 60439, USA*

[5]*Department of Physics, Graduate School of Science, Osaka University, 1-1 Machikaneyama, Toyonaka, Osaka 560-0043, Japan*

(Received 26 April 2012; revised manuscript received 11 July 2012; published 22 October 2012; corrected 4 January 2013)

We present *ab initio* calculations of magnetic exchange parameters of stoichiometric Heusler compound Ni_2MnSn and a few nonstoichiometric $Ni_2Mn_{1+x}Sn_{1-x}$ cases. Use of the exchange parameters in subsequent Monte Carlo simulations allows us to evaluate the magnetization curves as a function of temperature and composition as well as the critical temperatures of the magnetic phase transitions. The latter are compared to those obtained from a mean-field approximation using the Heisenberg model. We find that the variation of the experimental Curie temperatures of nonstoichiometric alloys can be explained theoretically if we assume that the main impact of disorder is the intermixing of manganese and tin on their corresponding sublattices and the simultaneous appearance of strong antiferromagnetic trends which originate from the nearest-neighbor Mn-Mn interactions on different sublattices. The Curie temperatures of the Ni-Mn-Sn alloys which have been obtained from the Monte Carlo simulations are in qualitative agreement with the experimental transition temperatures.

DOI: 10.1103/PhysRevB.86.134418 PACS number(s): 75.50.−y, 75.10.−b, 75.30.Sg

I. INTRODUCTION

The ferromagnetic (FM) shape memory materials of type Ni-Mn-X (X = In, Sn, Sb) have led to an existing field of research over the last decade because of the possible use of the diverse functionality of the alloys in different fields of technological applications.[1–5] Some interesting properties, such as magnetic shape memory effect (MSME), magnetic field induced strain (FIS), magnetoresistance (MR), exchange bias effect (EBE), and magnetocaloric effect (MCE), have been investigated for the nonstoichiometric Heusler alloys. As we know, the magnetic properties of these alloys are very sensitive to the content of Mn because the Mn excess atoms substitute for X on the X sublattice of the Heusler structure.

In the case of Ni-Mn-Sn alloys, the stoichiometric Ni_2MnSn compound orders in the $L2_1$ structure, in which the Sn atoms occupy the sites (0,0,0), Mn occupy $(\frac{1}{2},\frac{1}{2},\frac{1}{2})$ ones, and Ni atoms are located at the sites $(\frac{1}{4},\frac{1}{4},\frac{1}{4})$ and $(\frac{3}{4},\frac{3}{4},\frac{3}{4})$ with 16 atoms per unit cell.[6] In the nonstoichiometric case, $Ni_2Mn_{1+x}Sn_{1-x}$, we may assume that the excess Mn atoms occupy sites of the Sn-sublattice and that these atoms can interact antiferromagnetically (AFM) with the surrounding Mn atoms on the regular Mn sublattice because of the much shorter distance between Mn_1-Mn_2 compared to the Mn_1-Mn_1 and Mn_2-Mn_2 distances ("1" refers to the original Mn sublattice while "2" refers to the Sn sublattice).[6] Ferromagnetic behavior in the $L2_1$ structure is observed for the range $0.0 \leqslant x \leqslant 0.4$, and the Curie temperature, $T_C \approx 350$ K, is practically unchanged in this range of composition.[1–3] (For simplicity, we use here "$L2_1$" instead of B2 to designate the cubic austenitic Heusler structure and "$L1_0$" for the corresponding tetragonally distorted structure regardless of composition and c/a ratio.) The alloys with $0.4 < x \leqslant 1.0$ undergo a martensitic transition from the high-temperature $L2_1$ structure to the 10M, 14M, $L1_0$, or 4O structure depending on the composition.[5,7,8] These alloys show a variety of magnetic transitions. For Ni-Mn-X alloys, after the martensitic transformation, the Mn-Mn distance may decrease further due to the twinning in the martensitic phase which leads to enhanced antiferromagnetic (AFM) exchange interactions. The coexistence of FM and AFM interactions in the martensitic phase is also responsible for the EBE and inverse MCE.[9–14] For further features of the complex magnetic order of Heusler alloys (in relation to structural transformations and functional properties) we refer to the literature.[15–21]

The importance of the magnetic exchange interactions for the physical properties of the disordered Heusler materials was recently highlighted by Şaşıoğlu *et al.*[22] and Entel *et al.*[23] The dependence of the electronic structures, magnetic exchange parameters, and Curie temperatures of Ni_2MnX (X = Ga, In, Sn, and Sb) was investigated using different implementations of density functional theory (DFT) (augmented spherical wave method within the atomic-sphere approximation,[22] plane wave method as implemented in the Vienna *Ab initio* Simulation Package,[24] and the SPR-KKR-CPA method[25]). It was found that the magnetic exchange parameters show RKKY-like oscillatory behavior as a function of the interatomic spacing which however gets more and more disturbed with increasing amount of structural disorder. For example, in case of Ni_2MnSn the Mn-Mn exchange interactions increase within the first atomic shell compared to Ni_2MnGa and Ni_2MnIn while the exchange parameters within the third and fourth shells are small and strongly negative, respectively. Not only structural disorder is important but the addition of a quarternary transition element which has recently been discussed by Siewert *et al.* for the (Pt, Ni)-Mn-Z alloys with Z = Ga, Sn using DFT and Monte Carlo (MC) simulations.[26] The theoretical martensitic transition temperatures have been obtained from free-energy calculations involving phonons and DFT total energies, whereas the Curie temperatures have been calculated from MC simulations

 ©2012 American Physical Society

using the Heisenberg model with the *ab initio* exchange parameters.

The influence of configurational order and disorder in Heusler alloys based on the Co_2MnGa system was investigated theoretically by Singh *et al.*,[27] Arroyave *et al.*,[28] and Siewert *et al.*[29] using DFT calculations. The authors suggested that the austenitic and martensitic phases have disordered B2 structure. Ghosh and Sanyal discussed the influence of structural disorder in Ni-Mn-Ga alloys also using first-principles calculations.[30] The discussion of the different magnetic phases which emerge from the magnetic exchange interactions shows that structural disorder and increasing valence electron concentration leads to competing FM and AFM interactions which are present at all temperatures. However below the martensitic transformation temperature, the influence of the AFM interactions becomes overwhelmingly large. This is the characteristic feature of all alloys which emerge from the series Ni_2Mn_{1+x}(Ga, In, Sn, Sb)$_{1-x}$. This behavior is decisive since it influences mostly the various kinds of functional properties mentioned above. Another quite general observation is that the Ni-Mn exchange interaction is usually FM and helps to stabilize a FM ground state although the Mn-Mn interaction can be larger and AFM. Details of first-principles and MC simulations show that the actual magnetic spin configuration depends on composition, temperature, and whether the system is in the austenitic or martensitic phase.[23,31]

In this paper we report *ab initio* calculations of the magnetic exchange parameters and Monte Carlo simulations of the Curie temperatures of nonstoichiometrically ordered and disordered Heusler $Ni_2Mn_{1+x}Sn_{1-x}$ alloys. For some nonstoichiometrically disordered alloys we consider different degrees of disorder from 5% to 50% between Mn and Sn atoms. For example, 5% of disorder in Ni_2MnSn alloy means that 5% of the Sn atoms on the regular Sn sublattice are randomly replaced by 5% of Mn atoms, whereas 5% of Mn atoms at the regular Mn sublattice are randomly replaced by 5% of Sn atoms. Henceforth, we call this "structural disorder" to be distinguished from the "chemical disorder" in the case of Mn excess where the Mn excess atoms substitute Sn on the Sn sublattice (denoted as "nonstoichiometrically ordered"). We show that both types of disorder are required to explain the magnetic trends of the $Ni_2Mn_{1+x}Sn_{1-x}$ alloys in order to reproduce the experimental trends.

The magnetic exchange parameters are calculated for ordered ($L2_1$, 4O, and $L1_0$) structures and for such $L2_1$ structure in which partial disorder between Mn and Sn atoms exists. For the ordered and "disordered" $L2_1$ structures, we calculate the magnetization curves and plot the magnetic *T-x* diagram of $Ni_2Mn_{1+x}Sn_{1-x}$ alloys as it is obtained from the MC simulations and mean-field approximation (MFA) using the *ab initio* magnetic exchange parameters. Also, the MC simulations of the magnetization curves for the ordered and "disordered" $L2_1$ structure allow us to plot the composition-disorder phase diagram displaying ferromagnetic and antiferromagnetic (or ferrimagnetic) phases.

The paper is organized as follows. In Sec. II we discuss the results of *ab initio* calculations of the magnetic properties of ordered and disordered Ni-Mn-Sn systems. In Sec. III we present the results of Monte Carlo simulations. Concluding remarks are listed in Sec. IV.

II. *AB INITIO* CALCULATION OF THE MAGNETIC PROPERTIES OF $Ni_2Mn_{1+x}Sn_{1-x}$ ALLOYS

In this section, we present computational details of the calculation of magnetic exchange parameters, magnetic moments, and densities of states (DOS) curves for the ordered and disordered $Ni_2Mn_{1+x}Sn_{1-x}$ alloys. The calculations have been carried out for the high-temperature austenitic $L2_1$ structure (space group $Fm\bar{3}m$) and for the low-temperature martensitic 4O and $L1_0$ structures (space groups $Pmma$ and $Fmmm$, respectively). For the electronic structure calculations and evaluation of exchange parameters we used the spin-polarized relativistic Korringa-Kohn-Rostoker (SPR-KKR) code.[32] The effect of chemical disorder is taken by using the single-site coherent-potential approximation (CPA). The magnetic exchange parameters are calculated by using the formula from the Ref. 33 (see also Refs. 34 and 35),

$$J_{ij} = \frac{1}{4\pi}\int^{E_F} dE\ \mathrm{ImTr}\{\Delta_i \tau_\uparrow^{ij} \Delta_j \tau_\downarrow^{ji}\}. \tag{1}$$

τ is the scattering path operator and $\Delta_i = t_{i\uparrow}^{-1} - t_{i\downarrow}^{-1}$, where t is the scattering t matrix. For disordered systems, the scattering path operator in the single-site CPA expression,

$$\tau^{ij} = \left[1 + \tau_c^{00}\left(t_i^{-1} - t_c^{-1}\right)\right]^{-1} \times \tau_c^{ij}\left[1 + \left(t_j^{-1} - t_c^{-1}\right)\tau_c^{00}\right]^{-1}, \tag{2}$$

is substituted in Eq. (1). Here the exchange interaction between a pair of spins is projected onto the classical Heisenberg Hamiltonian. Since within this method the exchange parameters are computed from the total energy variation due to small rotations of a pair of spins causing a perturbation in spin density, it is obvious that structural disorder as well as changes of distance between the atoms due to martensitic transformations will greatly affect the magnetic exchange parameters J_{ij}.

As just mentioned, in this paper we include the effect of chemical disorder on the J_{ij} using the single-site CPA. The maximum number of CPA iterations and the CPA tolerance were set to 20 and 0.01 mRy, respectively. The first step in these calculations is to calculate the self-consistent potential (SCF). The l_{max} (the angular momentum expansion for the major component of the wave function) was restricted to two. For SCF cycles, the scattering path operator was calculated by the Brillouin zone (BZ) integration[36] with the special point method using a regular k-mesh grid of 22^3 with 834 k points. All calculations were converged to 0.01 mRy of the total energy. To achieve this convergence, we have used the BROYDEN2 scheme[37–39] (an iterative quasi-Newton method to solve the system of nonlinear equations) with the exchange-correlation potential of Vosko-Wilk-Nusair (VWN).[40] The BROYDEN2 scheme was started after a first iteration. The iteration depth for the BROYDEN algorithm was set to 40. For the SCF calculations the arclike contour path in the complex energy plane has been chosen as in approach of weakly bound states which are treated as core states. The upper end of the energy path E_{max} is set to the Fermi energy E_F. Regarding the real part of lowest energy value we have used the value of $E_{min} = -0.2$ Ry. The number of E-mesh points was set to 30. In order to achieve faster convergence, the SCF mixing parameter was set to 0.20. The maximum number of SCF

TABLE I. Lattice parameters (Å) of $Ni_2Mn_{1+x}Sn_{1-x}$ (Refs. 5,7, and 8).

Structure				$L2_1$				
x	0	0.1	0.2	0.27	0.3	0.33	0.37	0.4
$a = b = c$	6.046	6.034	6.024	6.009	6.005	6.002	5.998	5.995
Structure					4O			
x			0.43	0.48	0.52	0.55	0.59	
a			8.584	8.584	8.583	8.583	8.583	
b			5.602	5.602	5.602	5.602	5.601	
c			4.362	4.362	4.362	4.361	4.361	
Structure					$L1_0$			
x				0.8	0.85	0.9		
a				7.595	7.592	7.589		
b				7.595	7.592	7.589		
c				6.98	6.96	6.93		
c/a				0.919	0.916	0.913		

iterations was taken to 200. The self-consistent potential is then used to calculate the magnetic exchange parameters with the help of the KKR Green's function method and the formulation of Liechtenstein *et al.*[33] For that we have taken the spin-polarized scalar-relativistic (SP-SREL) Dirac-Hamiltonian with an orbital momentum cutoff of $l_{\max} = 2$ on a grid of 57^3, i.e., 4495 k points. As the solver for SP-SREL differential equations the Bulirsch-Stoer (BS) method[39] with a tolerance of 2×10^{-8} was used. The exchange coupling parameters are calculated with respect to the central site i of a cluster atoms with the radius $R_{\text{clu}} = \max|R_i - R_j|$. We have taken the radius of a sphere R_{clu} of 2.5. For the lattice parameters we have used the values from Refs. 5,7, and 8 which are listed in Table I.

The *ab initio* magnetic exchange parameters of the ordered structures of $Ni_2Mn_{1+x}Sn_{1-x}$ are presented in Fig. 1. We emphasize again that for the "ordered nonstoichiometric" structures the excess Mn atoms (x) substitute Sn atoms (chemical disorder) not to be confused with the structural disorder (y) which is defined here as an additional intermixing of Mn and Sn on the corresponding Mn and Sn sublattices with concentration y. Figure 1 clearly reveals that for the cubic $L2_1$ structure in the range of compositions $0 \leqslant x \leqslant 0.27$, Mn excess leads to an insignificant decrease of the Mn_1-Mn_1 and Mn_1-Ni interactions (Mn_1 and Mn_2 denote atoms on regular Mn and Sn sublattice sites, respectively), whereas the Mn_1-Mn_2 and Mn_2-Ni interactions are negligibly small. In contrast, in the range of compositions $0.28 \leqslant x \leqslant 0.4$, we notice a rapid change of magnetic interactions. For example, the Mn_1-Mn_1 (Mn_1-Ni and Mn_2-Ni) interaction is decreased (enhanced) with increasing Mn excess.

Moreover the Mn_1-Mn_2 interaction for alloys with $x \geqslant 0.28$ is predominantly of AFM type. It should be noted that alloys with $x \geqslant 0.28$ are closely in composition to the alloys which undergo a martensitic transformation. It turns out that in the case of orthorhombic structure (4O), the AFM Mn_1-Mn_2 interaction is largest compared to other structures (the modulated monoclinic structures are not considered). The Mn_1-Mn_1 interactions are practically zero. This behavior indicates that there is a crossover from ferromagnetism to antiferromagnetism with increasing Mn excess. As stated before, the AFM ordering with increasing content of Mn is connected with the decrease of nearest-neighbor Mn-Mn distances. As shown in Ref. 23, the binary alloy Ni-Mn is antiferromagnetic with a Néel temperature of 1075 K as obtained from MC simulations. We would like to point out that the large AFM interactions are also responsible for the rapid drop in the magnetization curves of Ni-Mn-Sn alloys at the structural phase transition which leads to EBE and the inverse MCE. It should also be noted that our theoretical magnetic exchange parameters for the Ni-Mn-Sn alloys are close to the values which were obtained previously by Şaşıoğlu[22] and Entel.[23]

Figure 2 shows the experimental and theoretical concentration dependence of the total magnetic moment per formula unit, μ^{tot}, for the cubic $L2_1$ structure of $Ni_2Mn_{1+x}Sn_{1-x}$ alloys in the range $0 \leqslant x \leqslant 0.4$. The experimental magnetic moments were taken from Ref. 8 (estimated from the spontaneous magnetization curves). Theoretical values of μ_{Mn_1}, μ_{Mn_2}, and μ_{Ni} have been calculated for the ordered structure of Ni-Mn-Sn using the SPR-KKR package. The total magnetic moment per formula unit of $Ni_2Mn_{1+x}Sn_{1-x}$ is given by

$$\mu^{\text{tot}} = 2\mu_{\text{Ni}} + \mu_{\text{Mn}_1} - x\,\mu_{\text{Mn}_2}. \tag{3}$$

In the expression for μ^{tot} we take into account that the magnetic moment of Mn_2 atoms located on the Sn sites in $Ni_2Mn_{1+x}Sn_{1-x}$ is antiferromagnetically coupled to the magnetic moments of the Mn_1 atoms on the Mn sites.[6,20,41] As shown in Fig. 2, the theoretical and experimental values of the magnetic moments decrease with increasing x. The theoretical data show a drop of the magnetic moment in the range $0.27 < x < 0.3$. This drop is cause by the strong AFM interaction between Mn_1 and Mn_2 atoms; see Fig. 1(e) which goes hand in hand with the martensitic transition in this range of compositions although the experimental data show that the structural transition occurs in samples with $x = 0.4$. Nonetheless, Fig. 2 suggests that the calculated magnetic moments are in rather good agreement with the experimental data. It should be noted that in the paper of Ito *et al.* it was

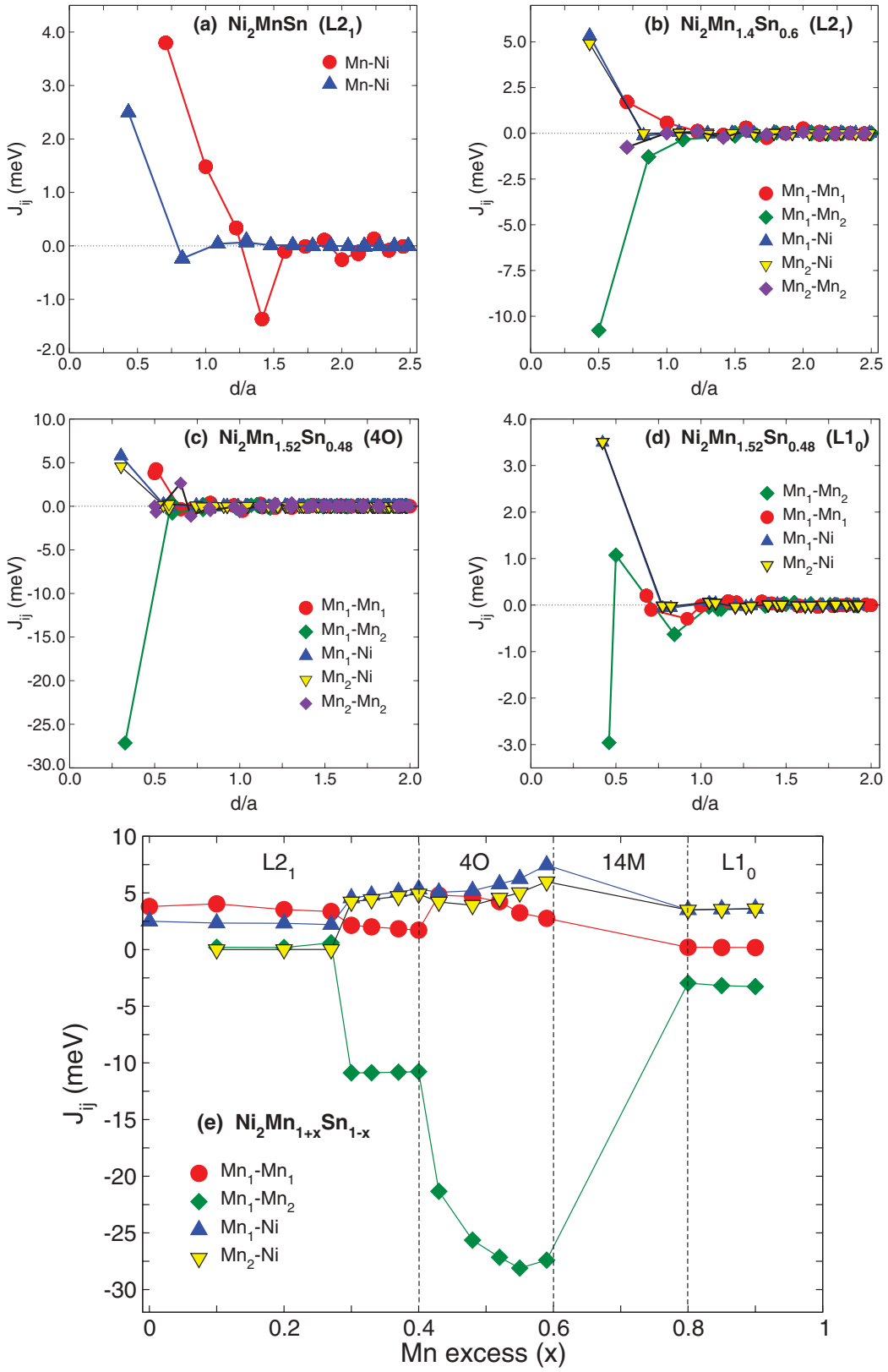

FIG. 1. (Color online) (a)–(d) The *ab initio* magnetic exchange parameters J_{ij} of $Ni_2Mn_{1+x}Sn_{1-x}$ for $x = 0, 0.4, 0.52, 0.8$ as a function of the distance d/a between the atoms in units of the lattice constant a. For instance, Mn_1-Mn_2 in the panel denotes the exchange interaction between the first atom (Mn_1) at the origin and the second atom (Mn_2) a distance d/a apart. (e) Composition dependence of magnetic exchange parameters in the first coordination shell of $Ni_2Mn_{1+x}Sn_{1-x}$.

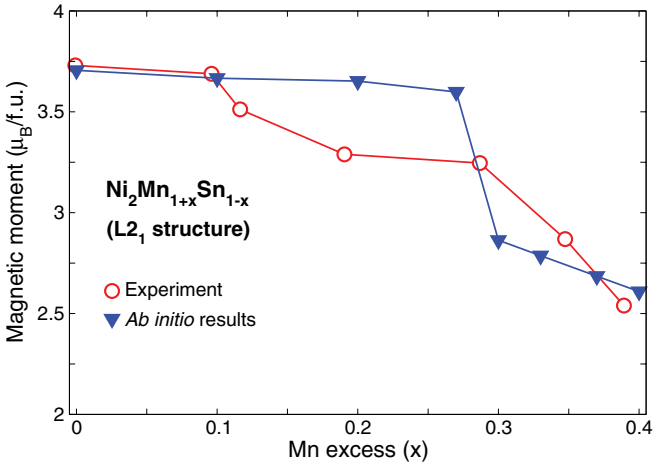

FIG. 2. (Color online) The experimental and theoretical (for the ordered structure) concentration dependence of the magnetic moment of $Ni_2Mn_{1+x}Sn_{1-x}$ alloys. The open (filled) symbols refer to the experimental (*ab initio*) data with experimental data from Ref. 8.

shown that the magnetic moment of $Ni_2Mn_{1+x}Sn_{1-x}$ first decreases with increasing x, reaches a minimum, and then increases again.[42] On the basis of our *ab initio* we cannot confirm that there is indeed such an intrinsic dependence.

We have also studied the influence of partial disorder between Mn and Sn atoms on the magnetic exchange parameters and magnetic moments of $Ni_2Mn_{1+x}Sn_{1-x}$. Figure 3 shows the dependence of the exchange parameters on the concentration of Mn excess and the disorder between Mn and Sn atoms. It should be noted that, for instance, a disorder of 10% means that 10% of regular Mn (Sn) sites are now occupied by the Sn (Mn) atoms which corresponds to a partially disordered B2 phase.

Clearly, the disorder has strong influence on the magnetic exchange parameters; see Fig. 3. We notice that first, the compositional dependence is rather smooth and second, the compositional range of rapid change of magnetic exchange parameters decreases with increasing disorder. For example, the Mn_1-Mn_1 interaction in Fig. 3(a) is reduced linearly with Mn excess due to increasing disorder. For 50% disorder and composition $Ni_2Mn_{1.4}Sn_{0.6}$ the Mn_1-Mn_1 interaction is approximately zero. This means that disorder destabilizes ferromagnetic order in cubic austenite of Ni-Mn-Sn and favors the appearance of strong AFM exchange between Mn_1-Mn_2 atoms in the whole concentration range of austenite ($0 \leqslant x \leqslant 0.4$), see Fig. 3(b), in comparison to the trend of Mn_1-Mn_2 interactions for the case of ordered structures. From Fig. 1(e) we may infer that the strong AFM exchange interaction is observed for the ordered systems only in the composition interval $0.27 < x \leqslant 0.4$. Further increase of disorder does not lead to a large decrease of the AFM exchange parameters. Figure 3(c) shows that for the case of ordered structures the Mn_2-Ni exchange is almost zero for the composition interval $0 \leqslant x \leqslant 0.27$. The increasing of disorder leads to the increasing of the Mn_2-Ni exchange [Fig. 3(d)]. On the other hand, it is obvious from Fig. 3(d) that the $Mn_1(Mn_2)$-Ni exchange increases linearly with increasing Mn excess and that the Mn_1-Ni and Mn_2-Ni exchange parameters are of the same magnitude for the ordered systems. Figures 3(e) and 3(f) show the dependencies of exchange parameters on the structural disorder (y) for $x = 0.21$ and 0.31. It is seen that the Mn_1-Mn_1 interactions almost linearly decrease with the increasing of the structural disorder, the $Mn_1(Mn_2)$-Ni exchange not depend on the disorder degree, and Mn_1-Mn_2 interactions depend nonlinearly on the structural disorder. The increasing of the AFM interactions with increasing of the structural disorder after 40% of the disorder can be explained by the increasing of the number of Mn_2 atoms on Sn sites.

We notice that for the case of ordered structures the Mn_1-Ni exchange practically does not change in the compositional range from 0 to 0.27, whereas the Mn_2-Ni interaction has practically zero value [Fig. 3(c)]. However, for the range $0.27 < x \leqslant 0.4$ this interaction rises sharply. The drop is due to the strong AFM exchange between Mn_1 and Mn_2; see Fig. 1(e). If we compare the exchange of $Mn_1(Mn_2)$-Ni for ordered and disordered cases, we notice that the exchange parameters of the ordered systems and disordered structures have the same slope in the range $0.27 < x \leqslant 0.4$.

In Fig. 4(a) we show the electronic density of states curves of $Ni_2Mn_{1.21}Sn_{0.79}$ for different degrees of disorder. We notice that for the ordered case the DOS curve is shifted as a whole to lower energies by $\approx$0.4 eV. We also observe that with increasing degree of disorder all peaks in the DOS curves are diminished. The DOS at the Fermi level of spin-down electrons is increased compared to the ordered case. For spin-up electrons the DOS at E_F does not depend much on the degree of disorder. Figure 4(b) shows the DOS curves for $Ni_2Mn_{1.31}Sn_{0.69}$. In this case the DOS curves for the ordered alloy are not shifted.

The value of the spin-down DOS at E_F of $Ni_2Mn_{1+x}Sn_{1-x}$ ($x = 0$–0.4) is plotted in Fig. 5 for different degrees of disorder (from 0% to 50%). The DOS value for the ordered alloy (0%) increases with increasing concentration and in the concentration range $0.27 \leqslant x \leqslant 0.29$ shows a jump followed by a constant value. This jump is caused by the strong AFM interaction between Mn_1 and Mn_2 atoms; see Fig. 1(e). If we allow for disorder then the jump is shifted to lower concentration. For 10% and higher disorder the jump has vanished and the DOS value increases monotonously, since in these cases the strong AFM interactions are observed in the whole composition range of $L2_1$ cubic structure as shown by our *ab initio* calculations [see Figs. 3(b) and 3(f)].

Figure 6 shows the theoretical dependence of the magnetic moment on excess Mn and disorder between Mn and Sn atoms in $Ni_2Mn_{1+x}Sn_{1-x}$. The behavior of μ^{tot} is presented in Fig. 6(a) while μ_{Mn_1} and μ_{Mn_2} are plotted in Fig. 6(b). In this case μ^{tot} per formula unit of the disordered $Ni_2Mn_{1+x}Sn_{1-x}$ alloys is given by

$$\mu^{\text{tot}} = 2\mu_{\text{Ni}} + (1-y)\mu_{\text{Mn}_1} - (y+x)\mu_{\text{Mn}_2} \qquad (4)$$

where y denotes the degree of structural disorder.

With increasing degree of disorder the total magnetic moment decreases smoothly with increasing x. For a large degree of disorder (more than 40%) the magnetic moment can even become zero or negative. This means that with increasing degree of disorder the alloy makes a transition to an antiferromagnetic (AFM) or a ferrimagnetic (FRM) state. This crossover has been discussed before. It is associated with

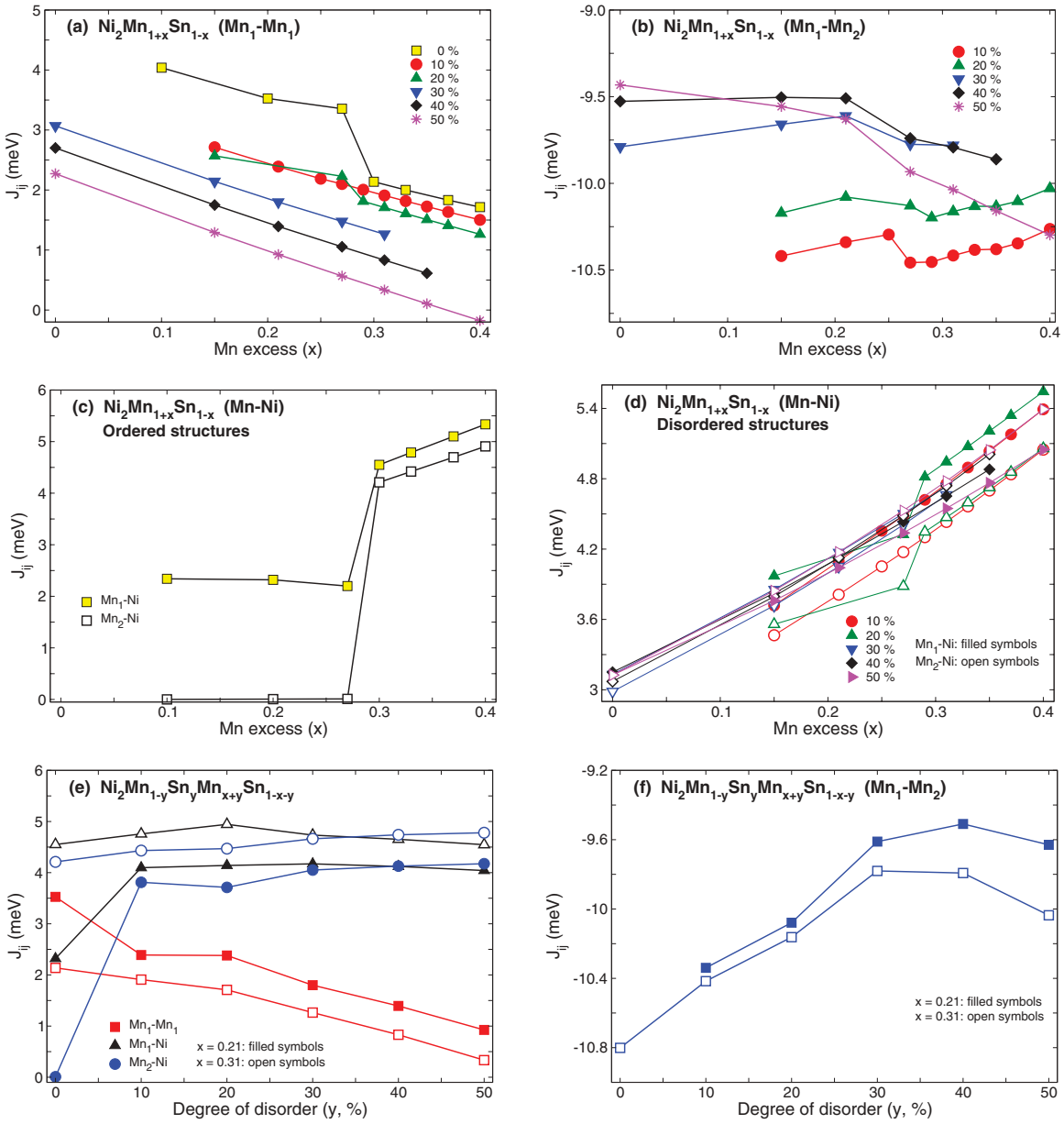

FIG. 3. (Color online) The dependence of the *ab initio* magnetic exchange parameters of the first coordination shell of $Ni_2Mn_{1+x}Sn_{1-x}$ on composition and disorder between Mn and Sn atoms. (a) The variation of the Mn_1-Mn_1 exchange parameters as a function of x for different degrees of disorder (y) ranging from zero to 50%. (b) The Mn_1-Mn_2 and (c) and (d) the Mn_1-Ni (filled symbols) and Mn_2-Ni (open symbols) exchange parameters. (e) and (f) The dependence of the exchange parameters from the degree of disorder for two compositions ($x = 0.21$ and $x = 0.31$).

the competition between ferromagnetic Mn_1-Mn_1, Mn_1-Ni, and Mn_2-Ni exchange interactions and the antiferromagnetic Mn_1-Mn_2 ones. It is well known that Mn which substitutes Sn becomes antiferromagnetically coupled to the surrounding Mn atoms which sit on the regular Mn sublattice. This allows us to describe the physics in terms of the first one being the Mn_1 sublattice and the second one the Mn_2 sublattice. With increasing degree of disorder the number of Mn atoms on the second sublattice increases but the magnetic moment (μ_{Mn_2}) of this sublattice decreases; see Fig. 6(b). The opposite situation is observed for the Mn_1 sublattice; here, the number of Mn atoms decreases with increasing disorder but the magnetic moment μ_{Mn_1} of this sublattice increases. At some degree of disorder the magnetic moments of both sublattices are equal and the alloy transforms to an antiferromagnetic state (for example, for composition $Ni_2Mn_{1.2}Sn_{0.8}$ with a degree of disorder of 40%). With further increase of disorder a ferrimagnetic state can be achieved with $\mu_{Mn_1} > \mu_{Mn_2}$ while the full magnetic moment of the alloy will be negative. This information may be used to derive from the MC simulations a compositional-disorder phase diagram for the $Ni_2Mn_{1+x}Sn_{1-x}$ alloys which is presented in the next section. We note that a similar tendency of the overall behavior of the magnetic moments has been observed experimentally and theoretically for the quaternary

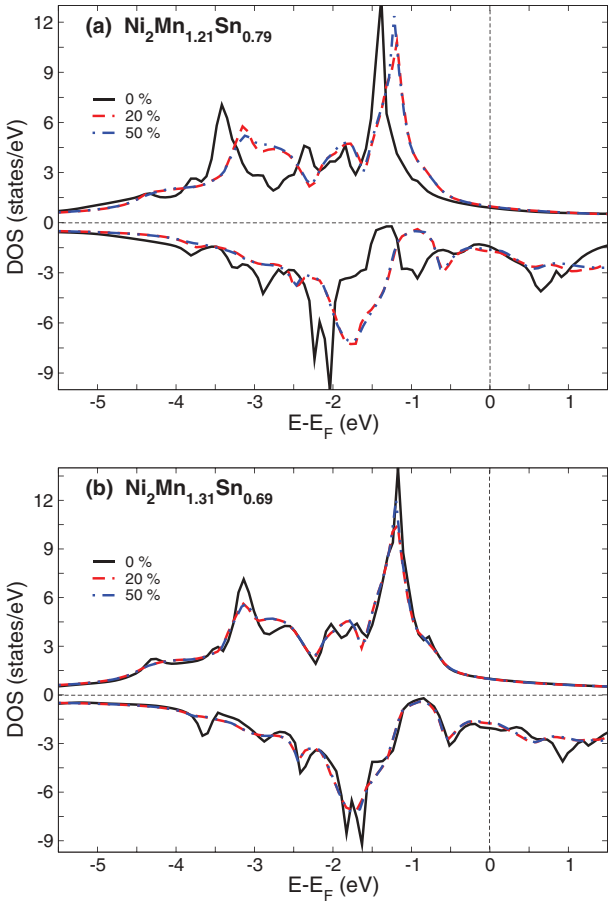

FIG. 4. (Color online) The total electronic DOS curves for the cubic structure of (a) $Ni_2Mn_{1.21}Sn_{0.79}$ and (b) $Ni_2Mn_{1.31}Sn_{0.69}$ with different degrees of disorder (y).

Heusler compound $Mn_{2-x}Co_xVAl$ with B2 order.[43] In this work the increase of Co content leads to a negative total magnetic moment and hence to the antiferromagnetic and ferrimagnetic order.

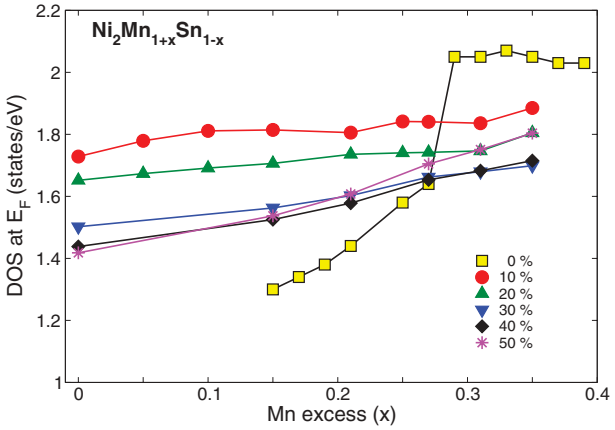

FIG. 5. (Color online) The compositional dependence of the spin-down DOS at the Fermi level of $Ni_2Mn_{1+x}Sn_{1-x}$ as a function of x and different degrees of disorder.

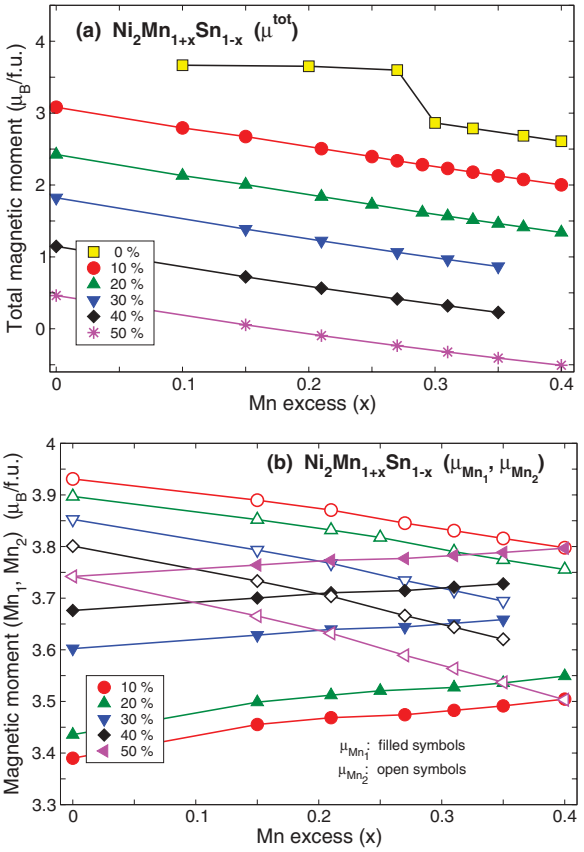

FIG. 6. (Color online) Theoretical magnetic moments per formula unit of $Ni_2Mn_{1+x}Sn_{1-x}$ as a function of the composition x and structural disorder (y) showing the (a) dependence of the total magnetic moment (μ^{tot}) and (b) dependence of the magnetic moments μ_{Mn_1} and μ_{Mn_2}. Lines with filled (open) symbols mark μ_{Mn_1} and μ_{Mn_2}, respectively.

III. EVALUATION OF THE COMPOSITION-DEPENDENT CURIE TEMPERATURES

In this section, we discuss the Curie temperatures of ordered and disordered $Ni_2Mn_{1+x}Sn_{1-x}$ alloys using the MFA and the MC simulations by employing the Heisenberg model.

The mean-field solution of the Heisenberg model has been obtained by diagonalizing corresponding matrices for the magnetic exchange parameters which can be obtained from the coupled equations for a multisublattice material.[22,27,44] We would like to remind the reader that the crystal structure of $L2_1$ Ni-Mn-Sn austenite consists of four interpenetrating fcc lattices A, B, C, and D with origin (A) at $(\frac{1}{2},\frac{1}{2},\frac{1}{2})$, (B) at $(\frac{1}{4},\frac{1}{4},\frac{1}{4})$, and (C) and (D) at $(\frac{3}{4},\frac{3}{4},\frac{3}{4})$ and (0,0,0), respectively. Mn and Sn occupy the A and D and Ni occupies the B and C sites. Since the excess Mn atoms are distributed randomly on the Sn sublattice, and Sn is assumed to be nonmagnetic, we consider a multisublattice Heusler system where Mn_1 (Mn_2) are located on sublattices A and D and two Ni sublattices B and C. The system of coupled equations (3)–(6) listed below has nontrivial solutions if the corresponding determinant is zero whereby the largest eigenvalue of the determinant determines

the Curie temperature:

$$\tfrac{3}{2}k_BTS_A = n_AJ_{AA}S_A + n_AJ_{AB}S_B + n_AJ_{AC}S_C + n_An_DJ_{AD}S_D, \quad (5)$$

$$\tfrac{3}{2}k_BTS_B = n_AJ_{BA}S_A + J_{BB}S_B + J_{BC}S_C + n_DJ_{BD}S_D, \quad (6)$$

$$\tfrac{3}{2}k_BTS_C = n_AJ_{CA}S_A + J_{CB}S_B + J_{CC}S_C + n_DJ_{CD}S_D, \quad (7)$$

$$\tfrac{3}{2}k_BTS_D = n_An_DJ_{DA}S_A + n_DJ_{DB}S_B + n_DJ_{DC}S_C + n_DJ_{DD}S_D. \quad (8)$$

Here, the J_{ml} $(m,l = A,B,C,D)$ represent the total sum of the *ab initio* exchange interactions between the m and l sublattices; n_m is the concentration of each atom in the non-stoichiometric Heusler alloys; S_m is the average z component of the spin.

For the $Ni_2Mn_{1+x}Sn_{1-x}$ alloys we have used the following parameters: $n_{Mn_1} = 1$, $n_{Mn_2} = x$ (where $x = 0 \ldots 0.4$). The summed values J_{mn} (where m, n = Mn_1, Mn_2, Ni) have been obtained from the SPR-KKR calculations. In order to check this method for nonstoichiometric Heusler alloys, we have simulated the concentration dependence of the Curie temperature of $Ni_{2+x}Mn_{1-x}Ga$ alloys for the cubic and tetragonal structures[45] as exemplary cases. We find that our Curie temperatures are in good agreement with other theoretical values which were obtained by Li *et al.*[44] For example, in the case of $x = 0$ (0.25) we obtain for the Curie temperature of austenite (T_C^A) and martensite (T_C^M, $c/a = 1.25$) $T_C^A = 435$ K and $T_C^M = 615$ K ($T_C^A = 286$ K, $T_C^M = 378$ K). Approximately, similar values have been presented by Li *et al.*[44] ($x = 0$: $T_C^A = 462$ K, $T_C^M = 658$ K, and $x = 0.25$: $T_C^A = 263$ K, $T_C^M = 362$ K). The small differences in Curie temperatures can be associated with the different methods when calculating the magnetic exchange parameters. In this context, we would like to point out that if we take into account two sublattices A and B, for example, for stoichiometic Ni_2MnGa (Ni_2MnSn), we obtain Curie temperatures very close to the experimental values, $T_C^A = 389$ K (Ga) [$T_C^A = 352$ K (Sn)], respectively (compare also Ref. 22). However, this is not completely accurate since we have to take into account the Ni sublattices as well (as is done here).

The Monte Carlo simulations have been performed for the real three-dimensional Heusler lattice using the Metropolis algorithm.[46] In its simplest version, some new, random spin direction is chosen and the energy change which would result if this new spin orientation is kept is then calculated. The number of sites is $N = L^3$, where L is the number of cubic unit cells of the Heusler alloys. We have used $L = 7$ which in the case of Ni_2MnSn leads to a simulation cell which contains 1687 Mn_1, 1688 Sn, and 2744 Ni atoms. The configurations of excess Mn_2 atoms on the Sn sublattice are chosen randomly and the total number of Mn_2 atoms is fixed by the composition $Ni_2Mn_{1+x}Sn_{1-x}$. In our MC simulations, we considered only magnetic interactions between magnetic Mn_1, Mn_2, and Ni atoms and have taken into account interactions within three coordination spheres. For example, each Mn_1 atom interacts with 42 Mn_1 atoms, 38 Mn_2 atoms, and 56 Ni atoms. The model Hamiltonian is written as

$$\mathcal{H}_m = -\sum_{\langle ij \rangle} J_{i,j}\,\mathbf{S}_i\mathbf{S}_j, \quad (9)$$

where the J_{ij} are the magnetic exchange parameters (positive in the case of FM interactions and negative in case of AFM interactions depending on the distance between the atoms); $\mathbf{S}_i = (S_i^x, S_i^y, S_i^z)$ is a classical Heisenberg spin variable $|\mathbf{S}_i| = 1$. The values of the magnetic exchange constants have been taken from our *ab initio* calculations.

As a time unit, we have used one Monte Carlo step consisting of N attempts to change the S_i variables. A new spin direction can be chosen by randomly choosing new spin components. The spin components are chosen in the following manner.[46] Two random numbers r_1 and r_2 are chosen from the interval [0, 1] to produce a vector with two components $\zeta_1 = 1 - 2r_1$ and $\zeta_2 = 1 - 2r_2$. The length of the vector is determined by $\zeta^2 = \zeta_1^2 + \zeta_2^2$ and if $\zeta^2 < 1$, then a new spin vector is computed with components

$$S^x = 2\zeta_1\sqrt{1-\zeta^2}, \quad (10a)$$

$$S^y = 2\zeta_2\sqrt{1-\zeta^2}, \quad (10b)$$

$$S^z = 1 - 2\zeta^2. \quad (10c)$$

For a given temperature the number of MC steps at each site was taken as 10^5. The simulation started from the ferromagnetic phase with $S_i^z = 1$. In order to obtain equilibrium values of the internal energy and order parameter, the first 10^4 MC steps were discarded. The internal energy of the system and the order parameter were averaged over 225 configurations for each 400 MC steps. The order parameter is defined in the following way:

$$m^\alpha = \frac{1}{N^\alpha}\sum_i \sqrt{\left(S_i^{\alpha,x}\right)^2 + \left(S_i^{\alpha,y}\right)^2 + \left(S_i^{\alpha,z}\right)^2}, \quad (11)$$

where α denotes Mn_1, Mn_2, and Ni and N^α the total number of α atoms; i runs over the corresponding lattice sites of the α atoms.

According to Eq. (4) the total magnetization for non-stoichiometric ordered $(y = 0)$ and disordered $(y \neq 0)$ $Ni_2Mn_{1+x}Sn_{1-x}$ alloys is calculated as

$$M = 2\mu_{Ni}\,m^{Ni} + (1-y)\mu_{Mn_1}\,m^{Mn_1} - (y+x)\mu_{Mn_2}\,m^{Mn_2} \quad (12)$$

with m^α given by Eq. (11). The dependence of the magnetic moments (μ_{Mn_1} and μ_{Mn_2}) on the composition and structural disorder allows us to derive the composition-disorder phase diagram of $Ni_2Mn_{1+x}Sn_{1-x}$ alloys (see Fig. 7) using the Heisenberg model and MC method.

The gray area in Fig. 7 marks the region of stable FM austenite with nonvanishing total magnetization given by Eq. (12) and finite Curie temperature, respectively. With increasing degree of disorder, i.e., with increasing intermixing of Mn and Sn on the corresponding Mn and Sn sublattices with concentration y (which can be described by $Ni_2Mn_{1+x}Sn_{1-x} = Ni_2Mn_{1-y}Sn_yMn_{x+y}Sn_{1-x-y}$ where x is the Mn excess concentration and y the degree of disorder), an AFM or FRM austenitic phase appears (white area). It is

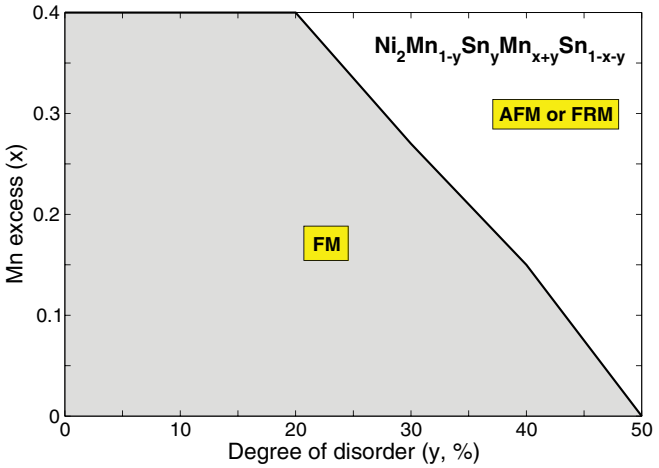

FIG. 7. (Color online) Calculated composition-disorder phase diagram of $Ni_2Mn_{1+x}Sn_{1-x}$ ($Ni_2Mn_{1-y}Sn_yMn_{x+y}Sn_{1-x-y}$). Here FM marks the region of the ferromagnetic phase while AFM and FRM denotes the antiferromagnetic or ferrimagnetic one.

interesting to note that for large disorder (y) and deviation from stoichiometric composition (x) we obtain $\mu_{Mn_1} > \mu_{Mn_2}$ [compare Fig. 6(b)], although the number of Mn_2 atoms may become larger compared to the number of Mn_1 atoms. This can lead to zero or negative values of the total magnetization although the sublattice magnetizations m^{Mn_1} and m^{Mn_2} are nonzero emphasizing the existence of an AFM or FRM phase.

Figures 8(a) and 8(b) show the magnetization curves of $Ni_2Mn_{1+x}Sn_{1-x}$ alloys for the cubic "$L2_1$" structure in zero magnetic field with degree of disorder (y) between Mn and Sn atoms ranging from 0% to 25%. Finally, Fig. 8(c) displays the experimental (T,x) phase diagram taken from Ref. 8 to which we have added the theoretical Curie temperatures.

Obviously, the experimental Curie temperatures (open circles) do not vary much with Mn excess up to $x = 0.5$. This is in contrast to the theoretical T_C values (filled circles) which decrease between $0 \leqslant x \leqslant 0.27$ in case of vanishing disorder, $y = 0$. This can be related to a slow reduction of the magnetic exchange interaction between Mn and Ni for this range of composition; see Fig. 1(e). For the subsequent range of compositions, $0.28 < x \leqslant 0.4$, we observe stronger interactions leading to an increase of $T_C(x)$. The same trend is found when using the mean-field approximation (filled diamonds). However, if we allow for disorder ($y = 25$ at. %) we can reproduce the approximately constant behavior of the experimental Curie temperatures in the compositional range $0 \leqslant x \leqslant 0.4$ (filled right triangles) which underlines the importance of intermixing effects in the Mn and Sn sublattices.

We have investigated the influence of disorder between Mn and Sn atoms on the Curie temperature more systematically. The Monte Carlo simulations of the Heisenberg model show that already for a disorder of 5% the Curie temperature is of the order of 400 K for all compositions from the interval $0.1 < x < 0.3$. Further increase of the degree of disorder leads to a small reduction of T_C. For $y = 0.5$–0.25, T_C practically does not change for compositions with $0 \leqslant x \leqslant 0.4$. The best agreement between theoretical and experimental results is

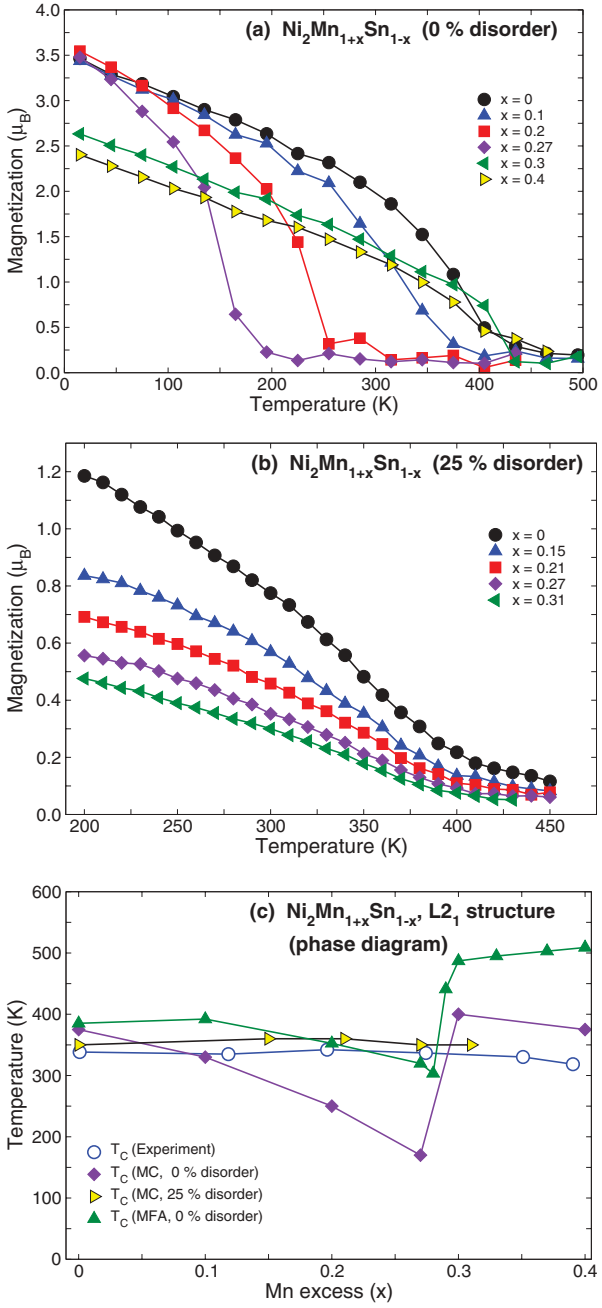

FIG. 8. (Color online) (a) Magnetization curves of $Ni_2Mn_{1+x}Sn_{1-x}$ ($0 \leqslant x \leqslant 0.4$) as a function of temperature in zero magnetic field and vanishing disorder ($y = 0$). (b) Magnetization curves of $Ni_2Mn_{1+x}Sn_{1-x}$ ($0 \leqslant x \leqslant 0.31$) in zero magnetic field for 25% disorder. (c) Experimental (T,x) phase diagram of $Ni_2Mn_{1+x}Sn_{1-x}$ to which the theoretical Curie temperatures have been added. The curves with open (filled) symbols mark the experimental (theoretical) data where the experimental data have been taken from Ref. 8.

obtained for a disorder of 25%; see Fig. 8(c). It should be noted we have also performed *ab initio* calculations of the magnetic exchange parameters and subsequent Monte Carlo simulations in order to obtain the Curie temperature for compositions with different disorder between Ni and Mn atoms. It seems that this type of intermixing is not realistic and does not

reflect the actual composition since in this case the calculated Curie temperatures deviate largely from the experimental ones. We tentatively conclude that structural disorder in Ni-Mn-Sn alloys involves primarily Mn and Sn on the corresponding two fcc sublattices.

IV. SUMMARY

We have investigated the effect of structural order and disorder on the magnetic properties of $Ni_2Mn_{1+x}Sn_{1-x}$ alloys in the concentration range ($0 \leqslant x \leqslant 0.9$) on the basis of density functional theory calculation and Monte Carlo simulations of the classical Heisenberg model. The magnetic exchange parameters and magnetic moments as well as the electronic structure and density of states curves have been determined by the *ab initio* calculations using the SPR-KKR package. The calculations reveal that strong AFM exchange interaction exists between nearest-neighbor Mn_1-Mn_2 atoms with Mn_1 located on the original Mn sublattice and Mn_2 on the Sn sublattice. This AFM interaction is important, i.e., particularly strong, in the region $0.27 < x \leqslant 0.4$.

The largest AFM interactions have been obtained for the martensitic phase of $Ni_2Mn_{1+x}Sn_{1-x}$ in the compositional range $0.4 < x \leqslant 0.6$. Any further increase of the Mn content leads to decreasing FM and AFM Mn-Mn exchange interactions.

It should be noted that the AFM Mn_1-Mn_2 interactions are predominant in tetragonally distorted $L1_0$-like martensite for the range $0.8 \leqslant x \leqslant 0.9$ where the FM Mn_1-Mn_1 interactions are approximately close to zero. This agrees with the experimental observation that the binary Ni-Mn alloy is antiferromagnetic. The calculations also show the important role of an additional degree of disorder between Mn and Sn (y) on the magnetic properties of $Ni_2Mn_{1+x}Sn_{1-x}$. This structural disorder in the $L2_1$ structure leads to strong AFM interactions between Mn_1 and Mn_2 in the composition range $0 \leqslant x \leqslant 0.4$. Moreover, with increasing x and y an AFM or ferrimagnetic austenitic phase is stabilized.

The Curie temperatures have been obtained from the MC simulations using the *ab initio* magnetic exchange parameters as input (in addition, we have calculated the magnetic transition temperatures using the MFA for the classical Heisenberg Hamiltonian by solving a matrix equation for the multisublattice system). The numerical results for the Curie temperatures in the case of structural disorder ($y = 0.25$) agree well with the experimental data.

We would like to point out that when taking into account the partially disordered B2 austenitic phase ($y \neq 0$), we find a stabilizing effect on the Curie temperature in the compositional range $0 \leqslant x \leqslant 0.4$. This is clearly in contrast to the case of an ordered $L2_1$ structure ($y = 0$) where both the MC simulations and MFA lead to drastic changes of the Curie temperature with increasing x. This means that partial structural disorder is one way to control the Curie temperature in some compositional range. We expect that this fact may be used to improve functional properties like the magnetic shape memory effect by, for example, appropriate alloying. On the other hand, the increase of AFM correlations may be used to enhance the magnetocaloric and exchange bias effects of the magnetic Heusler alloys.

ACKNOWLEDGMENTS

This work was supported by RFBR (Grants No. 11-02-00601 and No. 12-02-31129) and RF President Grant No. MK-6278.2012.2. P.E. acknowledges funding by the Deutsche Forschungsgemeinschaft (SPP 1239).

[1] Y. Sutou, Y. Imano, N. Koeda, T. Omori, R. Kainuma, K. Ishida, and K. Oikawa, Appl. Phys. Lett. **85**, 4358 (2004).
[2] X. Moya, L. Mañosa, A. Planes, T. Krenke, M. Acet, and E. F. Wassermann, Mater. Sci. Eng. A **438–440**, 911 (2006).
[3] L. Mañosa, X. Moya, A. Planes, S. Aksoy, M. Acet, E. F. Wassermann, and T. Krenke, Mater. Sci. Forum **583**, 111 (2008).
[4] A. Planes, L. Mañosa, and M. Acet, J. Phys.: Condens. Matter **21**, 233201 (2009).
[5] T. Krenke, M. Acet, E. F. Wassermann, X. Moya, L. Mañosa, and A. Planes, Phys. Rev. B **72**, 014412 (2005).
[6] C. V. Stager and C. C. M. Campbell, Can. J. Phys. **56**, 674 (1978).
[7] P. J. Brown, A. P. Gandy, K. Ishida, R. Kainuma, T. Kanomata, K.-U. Neumann, K. Oikawa, B. Ouladdiaf, and K. R. A. Ziebeck, J. Phys.: Condens. Matter **18**, 2249 (2006).
[8] T. Kanomata, K. Fukushima, H. Nishihara, R. Kainuma, W. Ito, K. Oikawa, K. Ishida, K.-U. Neumann, and K. R. A. Ziebeck, Mater. Sci. Forum **583**, 119 (2008).
[9] Z. D. Han, D. H. Wang, C. L. Zhang, H. C. Xuan, B. X. Gu, and Y. W. Du, Appl. Phys. Lett. **90**, 042507 (2007).
[10] V. K. Sharma, M. K. Chattopadhyay, R. Kumar, T. Ganguli, P. Tiwari, and S. B. Roy, J. Phys.: Condens. Matter **19**, 496207 (2007).
[11] P. J. Shamberger and F. S. Ohuchi, Phys. Rev. B **79**, 144407 (2009).
[12] V. D. Buchelnikov and V. V. Sokolovskiy, Phys. Met. Metallogr. **112**, 633 (2011).
[13] Z. Li, C. Jing, J. Chen, S. Yuan, S. Cao, and J. Zhang, Appl. Phys. Lett. **91**, 112505 (2007).
[14] H. C. Xuan, Q. Q. Cao, C. L. Zhang, S. C. Ma, S. Y. Chen, D. H. Wang, and Y. W. Du, Appl. Phys. Lett. **96**, 202502 (2010).
[15] V. V. Khovaylo, V. D. Buchelnikov, R. Kainuma, V. V. Koledov, M. Ohtsuka, V. G. Sharov, T. Takagi, S. V. Taskaev, and A. N. Vasiliev, Phys. Rev. B **72**, 224408 (2005).
[16] V. D. Buchelnikov, P. Entel, S. V. Taskaev, V. V. Sokolovskiy, A. Hucht, M. Ogura, H. Akai, M. E. Gruner, and S. K. Nayak, Phys. Rev. B **78**, 184427 (2008).
[17] S. Aksoy, M. Acet, P. P. Deen, L. Mañosa, and A. Planes, Phys. Rev. B **79**, 212401 (2009).
[18] T. Kanomata, Y. Kitsunai, K. Sano, Y. Furutani, H. Nishihara, R. Y. Umetsu, R. Kainuma, V. Miura, and M. Shirai, Phys. Rev. B **80**, 214402 (2009).
[19] V. V. Khovaylo, T. Kanomata, T. Tanaka, M. Nakashima, Y. Amako, R. Kainuma, R. Y. Umetsu, H. Morito, and H. Miki, Phys. Rev. B **80**, 144409 (2009).

[20]M. Ye, A. Kimura, Y. Miura, M. Shirai, Y. T. Cui, K. Shimada, H. Namatame, M. Taniguchi, S. Ueda, K. Kobayashi, R. Kainuma, T. Shishido, K. Fukushima, and T. Kanomata, Phys. Rev. Lett. **104**, 176401 (2010).

[21]M. Kataoka, K. Endo, N. Kudo, T. Kanomata, H. Nishihara, T. Shishido, R. Y. Umetsu, M. Nagasako, and R. Kainuma, Phys. Rev. B **82**, 214423 (2010).

[22]E. Şaşıoğlu, L. M. Sandratskii, P. Bruno, and I. Galanakis, Phys. Rev. B **72**, 184415 (2005).

[23]P. Entel, A. Dannenberg, M. Siewert, H. C. Herper, M. E. Gruner, V. D. Buchelnikov, and V. A. Chernenko, Mater. Sci. Forum **684**, 1 (2011).

[24]G. Kresse and D. Joubert, Phys. Rev. B **59**, 1758 (1999).

[25]H. Ebert, in *Electronic Structure and Physical Properties of Solids*, LNP Vol. 535, edited by H. Dreysse (Springer, Berlin, 1999), pp. 191–246.

[26]M. Siewert, M. E. Gruner, A. Dannenberg, A. Chakrabarti, H. C. Herper, M. Wutting, S. R. Barman, S. Singh, A. Al-Zubi, T. Hickel, J. Neugebauer, M. Gillessen, R. Dronskowski, and P. Entel, Appl. Phys. Lett. **99**, 191904 (2011).

[27]N. Singh, E. Dogan, I. Karaman, and R. Arroyave, Phys. Rev. B **84**, 184201 (2011).

[28]R. Arroyave, A. Junkaew, A. Chivukula, S. Bajaj, C. Yao, and A. Garay, Acta Mater. **58**, 5220 (2010).

[29]M. Siewert, M. E. Gruner, A. Danneberg, A. Hucht, S. M. Shapiro, G. Xu, D. L. Schlagel, T. A. Lograsso, and P. Entel, Phys. Rev. B **82**, 064420 (2010).

[30]S. Ghosh and B. Sanyal, J. Phys.: Condens. Matter **22**, 346001 (2010).

[31]V. D. Buchelnikov, V. V. Sokolovskiy, H. C. Herper, H. Ebert, M. E. Gruner, S. V. Taskaev, V. V. Khovaylo, A. Hucht, A. Dannenberg, M. Ogura, H. Akai, M. Acet, and P. Entel, Phys. Rev. B **81**, 094411 (2010).

[32]H. Ebert, D. Ködderitzsch, and J. Minár, Rep. Prog. Phys. **74**, 096501 (2011).

[33]A. I. Liechtenstein, M. I. Katsnelson, V. P. Antropov, and V. A. Gubanov, J. Magn. Magn. Mater. **67**, 65 (1987).

[34]I. Turek, J. Kudrnovský, V. Drchal, and P. Bruno, Philos. Mag. **86**, 1713 (2006).

[35]M. Ondráček, O. Bengone, J. Kudrnovský, V. Drchal, F. Máca, and I. Turek, Phys. Rev. B **81**, 064410 (2010).

[36]H. J. Monkhorst and J. D. Pack, Phys. Rev. B **13**, 5188 (1976).

[37]C. G. Broyden, Math. Comp. **19**, 577 (1965).

[38]G. P. Srivastava, J. Phys. A: Math. Gen. **17**, L317 (1984).

[39]W. H. Press, S. A. Teukolsky, W. T. Vetterling, and B. P. Flannery, in *Numerical Recipes in Fortran 77: The Art of Scientific Computing*, 2nd ed. (Cambridge University Press, Cambridge, 1992).

[40]S. H. Vosko, L. Wilk, and M. Nusair, Can. J. Phys. **58**, 1200 (1980).

[41]J. Enkovaara, O. Heczko, A. Ayuela, and R. M. Nieminen, Phys. Rev. B **67**, 212405 (2003).

[42]W. Ito, X. Xu, R. Y. Umetsu, T. Kanomata, K. Ishida, and R. Kainuma, Appl. Phys. Lett. **97**, 242512 (2010).

[43]M. Meinert, J.-M. Schmalhorst, G. Reiss, and E. Arenholz, J. Phys. D: Appl. Phys. **44**, 215003 (2011).

[44]C.-M. Li, H.-B. Luo, Q.-M. Hu, R. Yang, B. Johansson, and L. Vitos, Phys. Rev. B **82**, 024201 (2010).

[45]M. A. Zagrebin, V. V. Sokolovskiy, and V. D. Buchelnikov, Bulletin of Chelyabinsk State University, Physics **38**, 22 (2011).

[46]D. P. Landau and K. Binder, *A Guide to Monte Carlo Simulations in Statistical Physics* (Cambridge University Press, Cambridge, 2000).